CERN – EUROPEAN ORGANIZATION FOR NUCLEAR RESEARCH

CLIC-Note-733

ALIGNMENT TOLERANCES FOR THE CLIC DECELERATOR

E. Adli[*] **and D. Schulte**[**]

[*] University of Oslo and CERN

[**] CERN

Abstract

This note aims to quantify the alignment tolerances for the CLIC decelerator lattice elements by investigating the effects of wake fields and component misalignment. The tolerances comes from the requirements of transporting the entire beam through the lattice, while extracting the required amount of energy.

First, we briefly discuss the beam energy spread and its effect on the beam envelope. Then, we analyze the effects of the PETS dipole wakes for a perfect machine. Finally, the effect of lattice element misalignment is studied. Beam based alignment schemes for quadrupole correction will be presented, including modifications of the schemes needed for the CLIC decelerating station.

Simulations have been performed with the tracking code PLACET . The results indicate, for an energy extraction efficiency of 85%, that it would be possible to transport the entire decelerator beam through the lattice, if PETS misalignment are not larger than ~100 um and if beam based alignment methods are used for quadrupole correction.

Geneva, Switzerland
(28/02/2008)

Contents

1   Introduction

The purpose of the CLIC drive beam is to provide power for the CLIC main beam. Power is extracted from the drive beam using high-impedance Power Extraction Structures (PETS). The finite bunch length imply that the particles in a bunch will loose different amount of energy in each PETS, inducing an energy spread in the bunch, growing linearly with each PETS.

We have in this note tried to quantify the tolerances on the CLIC decelerator component misalignment. This has been performed by requiring transport of the entire beam through the decelerator station, while achieving the required power extraction at high efficiency.

1.1   Simulation set-up

The deceleration station simulated consists of 686 units - each containing two PETS, one quadrupole and one BPM (Figure 1). The PETS model implements the longitudinal monopole wake (energy loss) and the transverse dipole wakes (transverse kicks). The quadrupole field is linear. The BPM element has finite resolution (used for beam based alignment). Note that the lattice, including wakes, is *linear,* with uncoupled x and y planes. For more details, please refer to Appendix A.
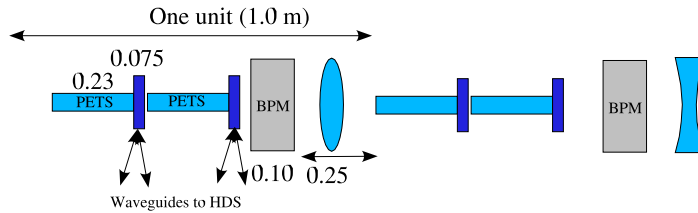
Figure 1: Deceleration lattice

1.2   Beam dynamics requirements

The main objective of the decelerator station is to **deliver the required power** to the accelerating structures of the main linac, timely and uniformly.

Furthermore, the **power production efficiency**, η, should be as high as possible. The efficiency is calculated as the ratio "energy of a drive beam pulse / power output to the accelerating structure at the operating frequency".

In order to ensure uniform power production along the lattice, the drive pulse must be transported through the whole station with **very small losses** (< 0.1 %).

Higher initial beam energy implies smaller beam envelope (higher rigidity and less adiabatic undamping), but also lower power production efficiency, giving conflicting requirements, as described in the next section. Also other requirements, like synchrotron radiation effects in the rings, turnarounds and bunch compressors put an upper limit on the energy.

2   Deceleration, beam envelope and metrics

2.1   Power extraction and longitudinal dynamics

The purpose of this section is not to give a full analysis of the decelerator longitudinal dynamics (this will be done in a future note), but to introduce the most relevant parameters for the study of the alignment tolerances.

With the CLIC parameters at the time of writing (see Appendix A) the PETS impedance and length were fixed: $\frac{R'}{Q} = 2294.7$ linac-Ohms, $\beta_g = 0.453$, $L_{PETS} = 23.1$cm [7]. The RF power generated by the bunched drive pulse can be expressed as

$$P = I^2 L_{PETS}^2 F(\sigma)^2 \omega_b \frac{R'/Q}{4v_g} = 149\text{MW} \tag{1}$$

where I is the average beam current, $F(\sigma)$ is the charge form factor[1], ω_b is the bunch frequency and $v_g = 0.453c$ is the group velocity of the fundamental longitudinal mode.

The wake generated in the PETS travels out of the PETS with group velocity v_g and is then coupled out and transferred to the accelerating structure. A bunch entering a PETS will catch up the field from n bunches ahead after travelling a distance $s = nd\beta_g/(1 - \beta_g)$, meaning that a bunch will feel the effect of the

$$n_{steady-state} = \left\lceil (\frac{l_{PETS}}{d}) \frac{(1 - \beta_g)}{\beta_g} \right\rceil = 12$$

leading bunches.

Figure 2 shows the longitudinal energy profile of the start of one train, after having passed through the decelerator station. In all plots the leading particles are to the left of plot. We observe how the train quickly reaches steady-state. Figure 3 shows the steady-state bunch energy profile. Notice how the energy minimum of the steady-state profile is not at the bunch centre, but shifted towards the back due to single-bunch wakes.
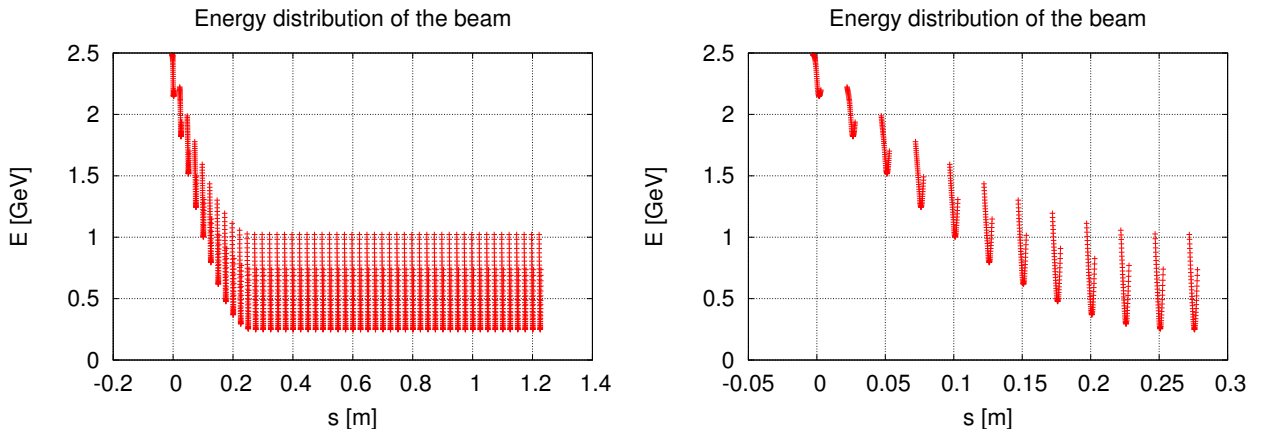

Figure 2: Energy profile of the beam

---

[1] $F(\sigma) = \int_{-\infty}^{\infty} dz' \cos kz' \frac{1}{\sqrt{2\pi}\sigma} \exp(-\frac{1}{2}(\frac{z'}{\sigma})^2) = e^{-\frac{1}{2}\sigma^2/\lambda^2}$, for a Gaussian bunch
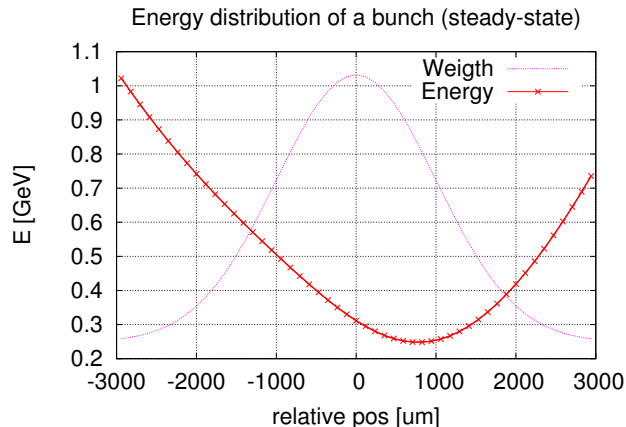
Figure 3: Energy profile of one steady-state bunch

For a given PETS, σ_z, and power requirements, the required current is uniquely determined by (1). The steady state power extraction efficiency, η, and the adiabatic beam envelope r_{ad} then depends on the initial drive beam energy E_0. The train extraction efficiency is defined as

$$\eta = \frac{E_{out}}{E_{in}} = \frac{PN_{PETS}}{IE_0/e}$$

and can be expressed as

$$\eta = S \times F(\sigma) \times \eta_{dist}$$

where S is the final energy spread (1 - minimum final particle energy / initial particle energy), $F(\sigma)$ is the bunch form factor, and η_{dist} is the reduction in efficiency due to the single-bunch wake effects. As a rule of thumb in this note we impose $S = 90\%$ in order to achieve an adequate beam envelope. However, it must be noted that one can in principle always trade lower η with smaller beam envelope by adjusting PETS and beam parameters.

The drive beam parameters for these simulations are :

P	147 MW	PETS power production, ss
I	96.4 A	Current
E_0	2.48 GeV	Initial beam energy
S	90.0 %	Maximum final energy spread, ss

2.2   Adiabatic undamping and resulting envelope

We define the 3σ beam envelope as $r = \max_i \sqrt{(|x_i| + 3\sigma_{x,i})^2 + (|y_i| + 3\sigma_{y,i})^2}$ (maximum along the lattice) [3], where x_i, y_i are the centroids of the macroparticles simulated. This might seem like a conservative way to measure the beam size, but is based on the requirement of loss-free beam transport. We define the beam envelope due to the adiabatic undamping alone as r_{ad} (perfect beam, perfect machine). Later, we will study the effects of component misalignment, and the total beam envelope will be composed of r_{ad} on top of the effects due to misalignments, as explained in the next section.
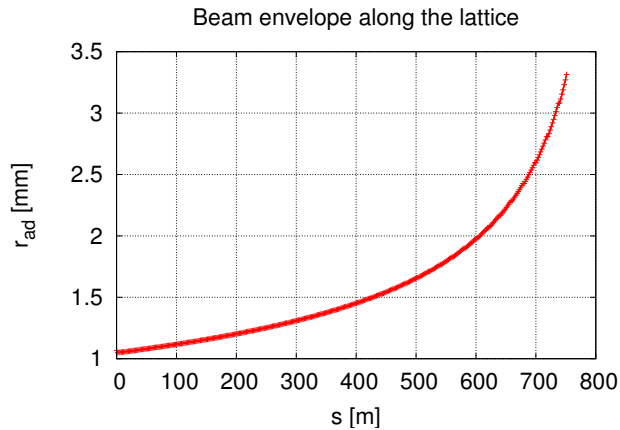
3

Figure 4: Beam envelope along lattice due to adiabatic undamping, r_{ad}

Figure 4 shows the beam envelope along lattice due to adiabatic undamping, with a resulting $r_{ad} = 3.2$mm (at the end of the lattice).

The adiabatic envelope, increasing with higher S (and η), can be expressed as (90° phase-advance assumed) :

$$r_{ad} = \sqrt{3^2 \sigma_x^2 + 3^2 \sigma_y^2} \approx 3 \cdot 2 \sqrt{L_{unit} \frac{\varepsilon_N}{(1-S)\gamma_0}}$$

2.3 Transverse metrics

Transverse wakes and misalignment will affect the macroparticle centroid motion along the linac. In order to separate this effect from the adiabatic undamping described above, we will for some of the simulations set the size of the distribution of each macroparticle to zero.

The largest centroid displacement for each machine will be found, and we define the metric, r_c, as the 90% percentile of the largest centroid displacement for N machines. Simulations with random scatter or jitter are normally run for 100 different random machines (see also the discussion in Appendix A.5). 90 out of 100 machines will then have an envelope smaller than r_c. An example of how simulation results of a 100 machines are distributed is shown in Figure 5. The envelope quoted for this example will thus be $r_c = 3.5$mm.
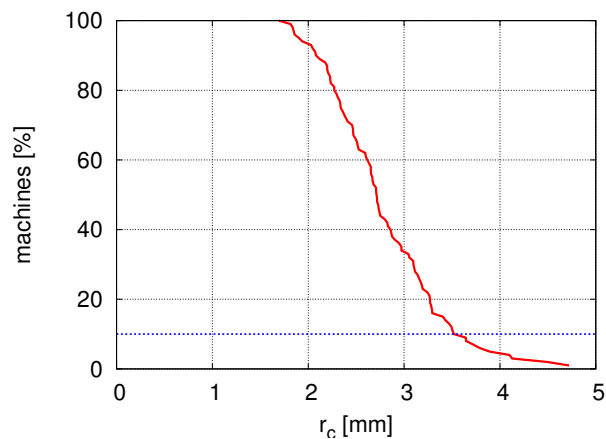

Figure 5: Example envelope distribution of 100 machines

4

The adiabatic envelope r_{ad} and r_c for the individual misalignment contribution will add to the total envelope. In the *worst* case we will have $r_{max} = r_{ad} + \Sigma_i r_{ci}$. In comparison, the PETS half-aperture is $a_0 = 11.5$mm. This gives an estimate of the maximum added envelope we can accept due to misalignment, and thus an estimate of accepted tolerances.

As a rule of thumb, each type of misalignment should give an $r_c \leq 1$mm, based on the fact that we get contributions from PETS x,y, PETS tilt x,y and quadrupole x,y.

We summarize our metrics in the following table (the metric used can be read off the axis in the graphs) :

Metric	Name	Explanation
r_{ad}	Adiabatic envelope	Beam envelope due to adiabatic undamping alone
r_c	Centroid envelope	Envelope of centroid particles
r	Total 3σ beam envelope	Total 3σ envelope (both ad. effects and centroid motion)

3 Beam envelope growth due to PETS wake fields

Before we investigate the effect of component misalignment and the corresponding tolerances, we investigate the beam envelope growth due to the PETS wakes for a perfect machine.

3.1 PETS transverse dipole kicks

PETS are high-impedance structures, producing strong wake fields in order to generate the required power. One of the main challenges of the PETS design is to prevent the transverse wake fields from inducing significant beam instabilities.

The PETS modeling and design for the current PETS design is described in [7]. The transverse dipole wake has been calculated and the most significant modes have been identified and included in the PLACET simulation (Appendix A).

For a given mode, the dipole wake function is 0 for $z > L(1 - \beta)/\beta$ (no time to catch-up) and for z$< L(1 - \beta)/\beta$:

$$W_\perp(z) = w\sin(\frac{\omega}{c}z)exp(-\frac{\omega z}{2Q(1-\beta)c})(1 - \frac{\beta}{L(1-\beta)})$$

where L is the PETS length. The transverse kick on a particle is given by the contribution of the wake from leading particles

$$\Delta y' = \sum_{modes} \sum_{particles} y_s \frac{q_s q_w}{E_w} L W_\perp(z) \tag{2}$$

where y_s is the transverse offset of the source particle inside the PETS.

3.2 Effect of dipole wakes in a perfect machine

In this section we study the effect of the transverse dipole wake kicks by simulating a perfect machine with jitter on the incoming beam. A more comprehensive review of the simulations performed is given in Appendix B.

We first investigate the amplification of the beam centroid if the initial beam has jitter induced at one given mode frequency, in order to study a particular mode individually. Figure 6 shows the amplification for each mode, for $Q = \{Q_0, 2Q_0, 3Q_0, 4Q_0\}$. We see that for the nominal PETS parameters the modes are well contained, but for a factor two larger Q, we start observing significant amplification of the centroid envelope.

To get an idea of how the combined modes add to the total beam envelope, we add beam jitter of one σ_y, distributed on the nine mode frequencies (for our parameters corresponding to 35μm per mode, superimposed. Larger jitter will lead to to a larger amplification of the total envelope). Figure 7 shows the total beam envelope. The graphs shows the cases with transverse wakes, $Q = Q_0$ and $Q = 2Q_0$, as well as the envelope without any transverse wakes ($w = 0$). We see, again, that for the nominal Q the amplification is small but that for $Q = 2Q_0$ the amplification becomes significant.
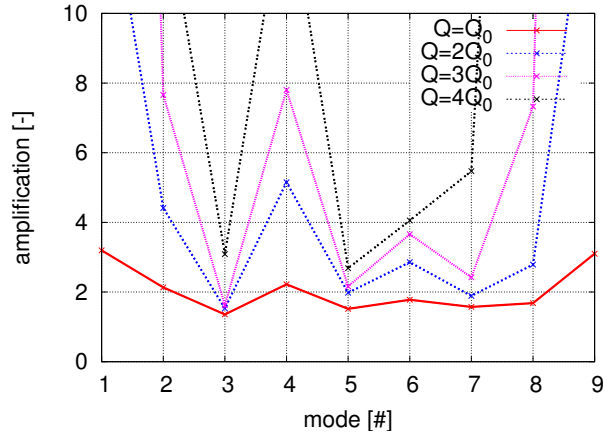
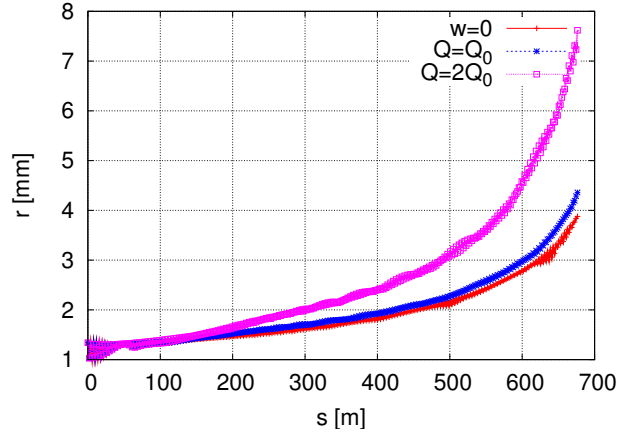Figure 6: Amplification of beam jitter due to transverse wake fields

Figure 7: Amplification of beam jitter due to transverse wake fields

3.2.1 Influence of the quality factor Q_i

Each wake mode is described by amplitude w_i, quality factor Q_i and frequency f_i[2]. We will show how the beam envelope depends on each of these parameters.

The quality factor, Q_i, determines how many bunches ahead are felt by a trailing bunch. It is considered difficult to predict the PETS Q-factor very accurately and therefore it would be of importance to have margin on the Q-factor. Figure 8 shows how the influence on the total envelope as the Q-factor of all modes are scaled simultaneously.

We observe that for Q of more than twice the nominal values leads to a very significant (> 2) amplification.

3.2.2 Influence of the wake amplitude w_i

The kicks are proportional to the mode amplitude, w_i. Large deviation from the calculated w_i is not expected, as this number depends mainly on the PETS aperture, but we include this analysis

---

[2]Each mode is also characterized by its group velocity β_i. In the current PETS model, however, corresponding modes with $\beta_i \to 0$ are used.
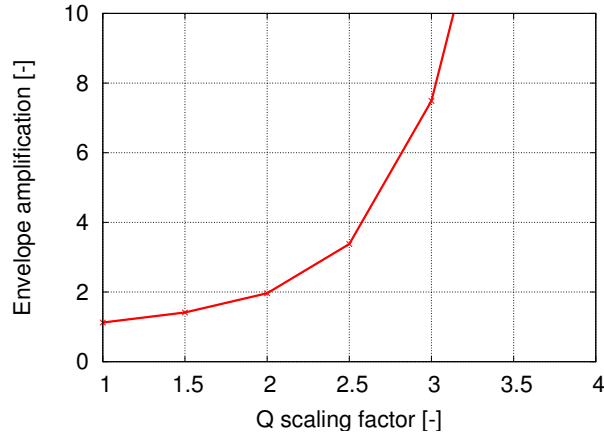
Figure 8: PETS wake field jitter amplification, varying Q

for completeness. Figure 9 shows how the influence on the total beam envelope as the w-value for all modes are scaled simultaneously.
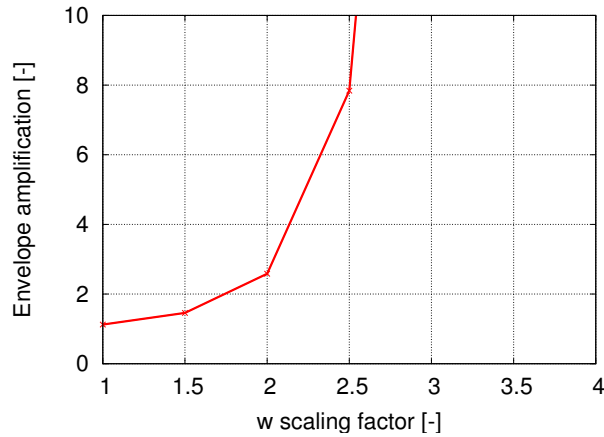
Figure 9: PETS wake field jitter amplification, varying w

3.2.3 Influence of the frequency f_i

The mode frequency is very significant, because if $f = \frac{n}{2}\frac{c}{d}$ (with d the bunch distance), trailing bunches will be on a zero-crossings and the kick will be very small (zero in the case of a point like bunch), while for f between zero-crossings the kicks will be large.

This is illustrated in Figure 10, showing the PETS modelled with one mode dipole with varying frequency (using resultant amplitude and damping: $w = 8.3V/pC/m/mm$, $Q = 4.6$).

Figure 10: PETS wake field jitter amplification, varying f

4 The effect of component misalignment

We want to study the effect of component misalignment on the beam envelope. The effects of misalignment of the individual component type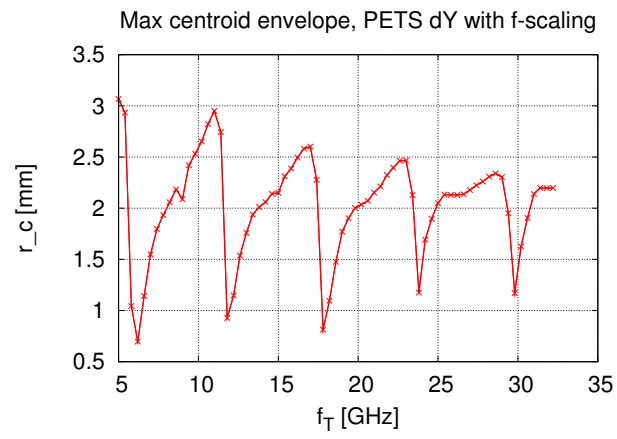s (PETS, Quadrupole, BPM) will be studied individually. In order to compare effects we will find the limit which gives a centroid envelope of 1mm (please refer to Section 2.3 for more details about the metrics used).

4.1 PETS

4.1.1 PETS misalignment

The dipole wake is proportional to source particle offset wrt. the PETS centre and the transverse kicks will therefore grow linearly with PETS transverse misalignment. One of the major design drivers for the PETS is to minimize the transverse dipole wakes, but there will always be some wake remaining. There are no mechanisms foreseen to mitigate further the resulting PETS kicks, and the PETS misalignment must therefore be kept small in order to avoid large kicks and beam envelopes

In order to study the effect of PETS misalignments individually, a beam is tracked through an otherwise perfect machine with the PETS scattered with an rms offset of σ_{PETS}. The resulting centroid envelope as function of σ_{PETS} is shown in Figure 11. We also also include results for PETS with scaled Q-factors. We note that the amplification due to larger Q is much less significant than in the previous section, since the beam offset is now induced by the misalignments and the transverse modes are not driven the mode resonantly.

PETS angle offset An small angle error, $\sigma_{\theta - PETS}$, in the PETS orientation will, in our linear model, have similar effect as the position offset, σ_{PETS}, given by $\sigma_{\theta, PETS} = 2(\sigma_{PETS} / \frac{1}{2} l_{PETS})$, as illustrated in Figure 11.
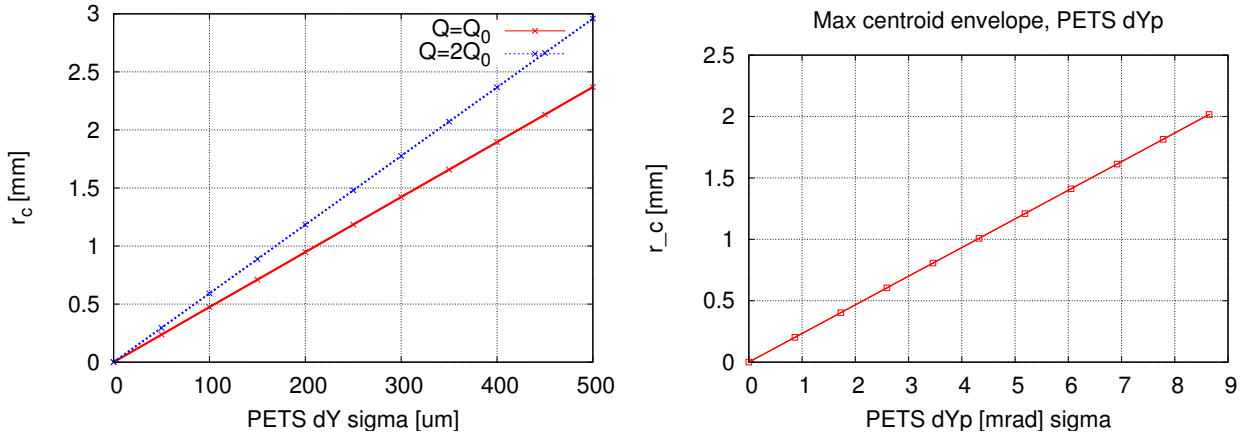

Figure 11: Effect of PETS misalignment, position and angle

1mm centroid offset corresponds to PETS misalignment of $\sigma_{PETS} \approx 200 \mu$m and $\sigma_{PETS,\theta} \approx$ 4mrad. If we want to allow for some margin on the wake parameters (Q and w) we would rather require $\sigma_{PETS} = 100 \mu$m.

4.2   Quadrupoles

A quadrupole offset will add a dipole component in the lattice, resulting in transverse kicks

$$\Delta y' = -\frac{\Delta y}{f}$$

It is foreseen that the quadrupoles and BPMs can be pre-aligned at best to a positioning accuracy of $\sigma_{BPM,quad} \sim 20\mu$m [6]. The effect on the remaining imperfections is studied here.

In order to study the effect of quadrupole misalignment individually, an ideal beam is tracked through an otherwise perfect machine.

4.2.1   Quadrupole misalignment

Position misalignment   Quadrupole vertical position is scattered with an rms offset of σ_{quad}, and the resulting beam envelope is shown in Figure 12.
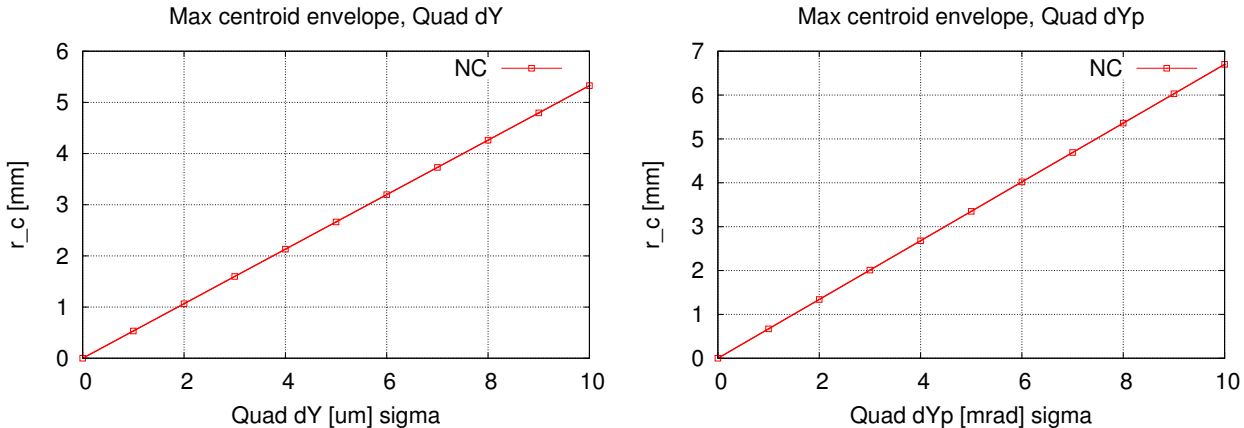

Figure 12: Effect of quadrupole misalignment, position and tilt

We see that for quadrupole offsets of few μm the increase in beam envelope is substantial, and the imperfections after pre-alignment will clearly be unacceptable for operation of the drive beam. Correction schemes for the quadrupoles are thus necessary, as discussed in Section 5. In order to limit the losses while tuning-up the machine and performing the alignment it is important the quadrupoles are pre-aligned as well as possible.

Angle errors   We also study the effect of quadrupole roll and tilt (applied to an otherwise perfect machine). From Figure 12 we note that the requirement on quad tilt offset precision is not too severe (as expected since to first order the effect will cancel out), giving a tolerance of $\sigma_{quad,\theta} \lesssim 1$mrad. Similarly, quadrupole roll simulations show that $\sigma_{quad,\psi} \lesssim 1$mrad will be more than adequate.

5   Beam-based alignment

Section 4.2.1 shows that the remaining static imperfections of quadrupoles after pre-alignment leads to a beam envelope much larger than what is acceptable. Correction strategies are therefore needed. As correctors one can either use correction coils for each quadrupole or one can put the quadrupoles on movers. In the ideal case the two approaches are mathematically equivalent. In these simulations, we assume quadrupole on movers.

We will first discuss the algorithms proposed for the decelerator station, then we apply them for the static case and we also verify some dynamic effects. In the simulations we assume a perfect incoming beam.

5.1   The response matrix

We introduce the response matrix in order to explain the algorithms used for the beam-based alignment schemes (1D-case shown for simplicity).

The corrector-to-BPM response matrix, $\mathbf{R}$, is defined as the trajectory shift inside the BPMs produced by a incremental change in the corrector magnets (in our case: incremental shift in quadrupole position)

$$dy_i = R_{ij}d\theta_j$$

where $\boldsymbol{\theta}$ is the corrector vector and $\mathbf{y}_i$ is the vector of BPM readings of a pulse tagged i.

5.2   1-to-1 correction

The most simple correction scheme, "1-to-1 correction", consists of moving each quadrupole individually so that the beam centroid goes through the centre of the following BPM. Since the BPM will not be perfectly aligned either, the transverse kicks will now depend on the BPM offsets.

5.2.1   Implementation of 1-to-1 correction

In terms of the response matrix the 1-to-1 correction scheme can be described as follows:

1. Send a pulse through the lattice

2. Record the BPM readings $\mathbf{y}_0$

3. Adjust the quadrupole positions according to

$$\Delta\theta = -\mathbf{R}_0^\dagger\mathbf{y}_0$$

where $\mathbf{R}_0^\dagger$ denotes the least-squares inverse. Any subsequent pulse, with the same pulse characteristic, will go through the BPM centers.

5.2.2 Simulation results

Simulation of 1-to-1 correction with perfectly aligned BPMs shows, as expected, a perfect result independend of the quadrupole error.

In order to show the performance of 1-to-1 correction wrt. to no correction, we assume the pre-alignment limit for the BPMS, $\sigma_{BPM} = 20\mu$m [5]. The resulting r_c as function of σ_{quad} is shown for the two cases is shown in 13 ("NC" stands for "No Correction"). We see that for the case of equal misalignment for the quads and the BPMs, $\sigma_{BPM} = \sigma_{quad}$, we would still get a factor 3 improvement with 1-to-1 correction wrt. to no correction.

However, due to the energy spread and the phase-space dilution, the resulting beam envelope for $\sigma_{BPM} = 20\mu$m, $r_c = 3.5$mm, is still not acceptable for routine operation of the CLIC deceleration, implying a need for more advanced alignment schemes.
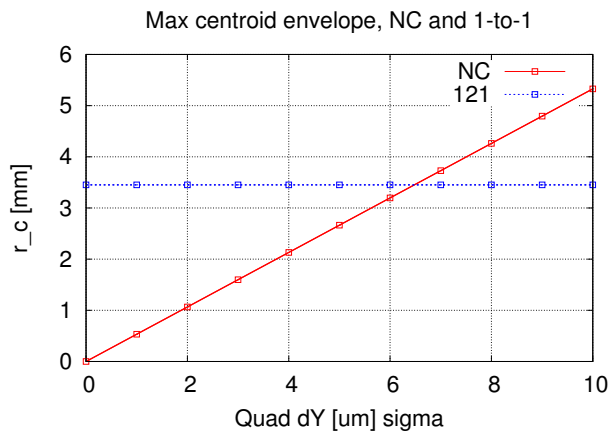

Figure 13: 1-to-1 correction ($\sigma_{BPM} = 20\mu$m)

5.3 Dispersion Free Steering

The correction scheme Dispersion Free Steering (DFS) is based on the following idea: the dipole components induced by the quadrupole misalignment introduces dispersion (energy dependent trajectories) in the lattice. If one sends beams with different energies wrt. to the optics through the lattice, one will observe different trajectories. By adjusting the quadrupole position such that the trajectories be the same, one can eliminate the harmful components of the quadrupole misalignment.

5.3.1 Implementation of DFS

In principle this can be achieved by first sending one pulse with e.g. the nominal energy - the "main pulse" - and store the BPM positions along the lattice, $\mathbf{y_0}$. Then, sending a second pulse, with a different energy[3] - the "test pulse" - and again store the BPM positions, $\mathbf{y_1}$. Then, one seek to minimize the difference in BPM readings $(\mathbf{y_1} - \mathbf{y_0})$. However, such a strategy is unstable

---

[3]alternatively, one could use pulses with the same energy, and adjust the lattice focusing strength instead.

in presence of non-zero noise, for example due to finite BPM resolution σ_{res}. To overcome this problem, one instead weights the difference $(\mathbf{y}_1 - \mathbf{y}_0)$ with a requirement that the beam go through centre of the BPMs (as in 1-to-1 steering). Mathematically we want to minimize the metric function

$$\chi^2 = w_0 \Sigma y_{0,i}^2 + w_1 \Sigma (y_{1,i} - y_{0,i})^2$$

This is an over-constrained system. The least squares solution, wrt. the correctors, is found by solving the resulting matrix equations :

$$\frac{d\chi^2}{d\boldsymbol{\theta}} = \frac{d}{d\boldsymbol{\theta}} w_0 (\mathbf{y}_0 - \mathbf{R}_0 \Delta\boldsymbol{\theta})^T (\mathbf{y}_0 - \mathbf{R}_0 \Delta\boldsymbol{\theta}) + w_1 ((\mathbf{y}_1 - \mathbf{y}_0) - (\mathbf{R}_0 - \mathbf{R}_1)\Delta\boldsymbol{\theta})^T ((\mathbf{y}_1 - \mathbf{y}_0) - (\mathbf{R}_0 - \mathbf{R}_1)\Delta\boldsymbol{\theta}) = 0$$

$$\Rightarrow \left[\begin{array}{c} \sqrt{w_0}\mathbf{y}_0 \\ \sqrt{w_1}(\mathbf{y}_1 - \mathbf{y}_0) \end{array} \right] = \left[\begin{array}{c} \sqrt{w_0}\mathbf{R}_0 \\ \sqrt{w_1}(\mathbf{R}_1 - \mathbf{R}_0) \end{array} \right] \Delta\boldsymbol{\theta}$$

$$\Rightarrow \Delta\boldsymbol{\theta} = \left[\begin{array}{c} \sqrt{w_0}\mathbf{R}_0 \\ \sqrt{w_1}(\mathbf{R}_1 - \mathbf{R}_0) \end{array} \right]^{\dagger} \left[\begin{array}{c} \sqrt{w_0}\mathbf{y}_0 \\ \sqrt{w_1}(\mathbf{y}_1 - \mathbf{y}_0) \end{array} \right]$$

Large BPM offset, σ_{BPM}, suggests to use a relatively lower w_0 while poor BPM resolution, σ_{res}, suggests to use a relatively lower w_1. The relative weighting should be in the order $w_1/w_0 = \sigma_{BPM}^2/\sigma_{res}^2$. Optimal weighting is found by simulation.

For long lattices, one will in practice group correctors in bins, and apply DFS to each bin, with eventual bin overlap. For realism, PLACET also performs such binning. Finally, in our model is linear, but in the case of significant non-linearities in the system, the DFS-procedure will require several iterations to converge. Please refer to Appendix C for further details about the DFS and the parameters used in the following simulations.

5.3.2 Drive Beam issues: current test beam versus energy difference

This implementation of dispersion free steering requires an energy difference between the main and test pulses in order to generate the different trajectories. For the CLIC main beam one uses test beams with different energy, produced by either varying the RF phase in the bunch compressor or changing the structure gradient [2].

However, for the drive beam this is problematic: a test beam with lower energy than the nominal will not be well focused, because the lattice focusing will be optimized so that the lowest energy particles are well focused [1]; while a test beam with higher energy than the nominal is not foreseen to be available.

Instead, one can use a test beam with a lower current to produce the dispersive trajectory, because the PETS will decelerate the lower current beam less, resulting in a test beam with higher energy. This is shown in Figure 14; a lower energy beam results in a blow-up of the beam envelope, while a lower current beam results in a stable beam, thus fit for dispersion free steering.

 The low current can either be produced by reducing the bunch charge (more awkward in practise), or taking out a pattern of bunches from the train (considered easier). The last approach is the one used in the DFS simulations below, with a beam as shown in Figure 15 (1/3 of bunches removed). Which bunches are removed does not affect the result significantly (e.g. removing every third bunch instead gives similar results). For more details about the DFS setup, please refer to Appendix C. In this note we have not investigated in detail the losses of the test-beam in the decelerator, this will be done in a future note on decelerator operation and tune-up.
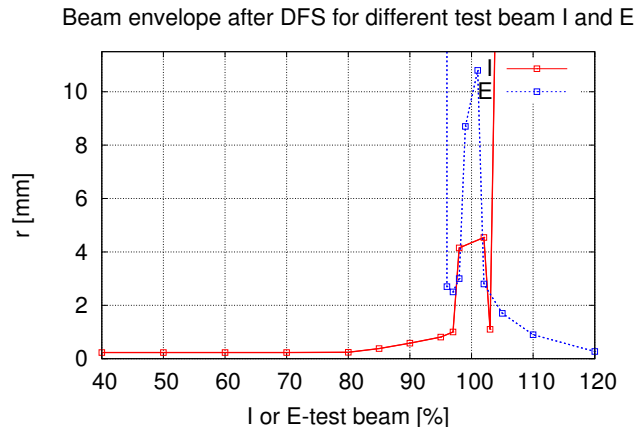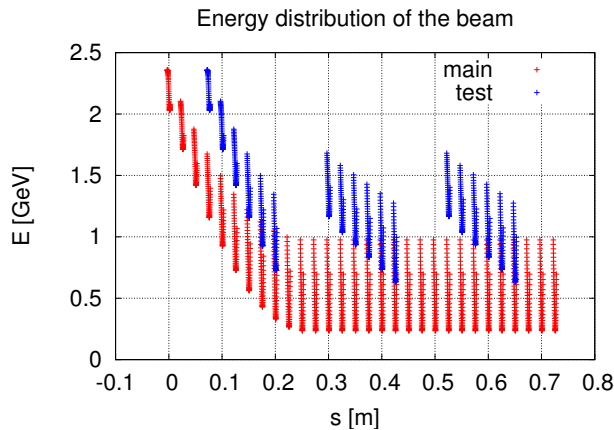
Figure 14: Energy versus current test beams

Figure 15: Test beam and energy profiles of main test beam

5.3.3 Simulation results

The results of the dipersion free steering algorithm are independent of initial values of σ_{quad}, but depends on both σ_{BPM} and σ_{res}. We assume also here the pre-aligment limit of $\sigma_{BPM} = 20\mu$m. Figure 16 shows the resulting r_c after performing dispersion free steering, as function of BPM resolution.

Dynamic jitter Tolerances for dynamic effects (originating e.g. from ground motion) are known to be very strict for the main linac (order of magnitude few 10's of a nanometer [2]).

The effect of dynamic jittering of the quadrupoles were investigated for the decelerator lattice. Dispersion free steering was applied, but with the quadrupoles jittered, with rms σ_{jit}, during the algorithm (jitter was applied bin by bin, between two shots)

Jitter from $\sigma_{jit} = 100nm$ up to $\sigma_{jit} = 1\mu$m were applied, with negligible effect on the beam envelope in all cases. The reason is that our metric, the envelope, is measured in mm while the main linac metric, the emittance, is measured in nm.
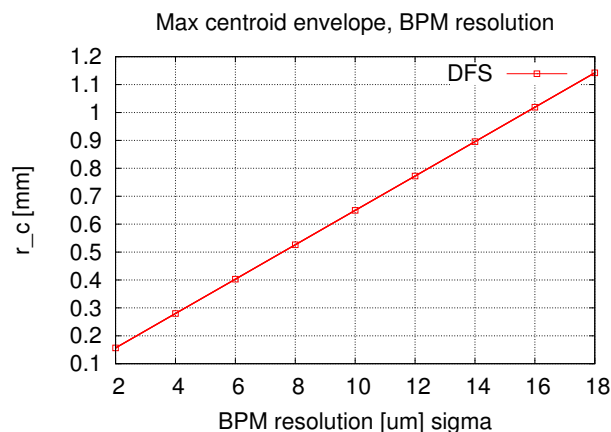
15

Figure 16: Dispersion free steering

5.4 Summary of the effect of beam based alignment

We observe the results with no correction, 1-to-1 correction and DFS in Figure 17. We sum up:

- Without correction the beam envelope for $\sigma_{quad} = 20\mu$m is very large, and therefore beam-based alignment must be performed

- The quadrupoles must still be pre-aligned as well as possible in order to limit the losses when tuning-up and performing alignment

- 1-to-1 steering implies that the quadrupole misalignment, σ_{quad}, is corrected, and only the BPM misalignment, σ_{BPM}, is of importance. The resulting envelope depends linearly on σ_{BPM}

- Even with a pre-alignment of $\sigma_{BPM} = 20\mu$m the beam envelope is too large for operation and more performant alignment schemes are therefore needed

- With dispersion free steering the results from 1-to-1 steering can be improved further with a sufficient good σ_{res}. The resulting beam envelope depends linearly on σ_{res}
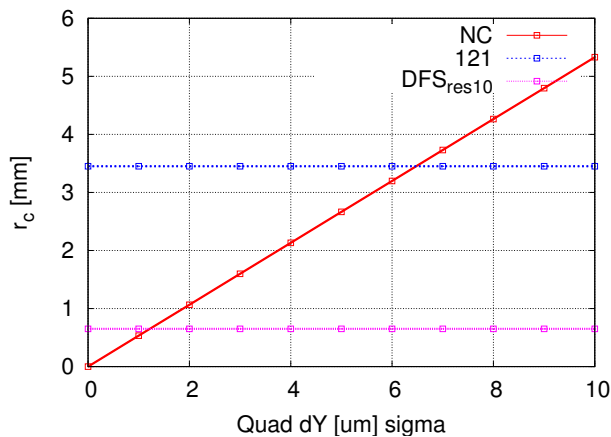

Figure 17: No correction, 1-to-1 correction and DFS ($\sigma_{BPM} = 20\mu$m and $\sigma_{res} = 10\mu$m)

16

We note that the dispersion free steering works very well for our model after only one iteration, but this is not surprising since our lattice is fully linear. For more accurate results one might have to add non-linear effects as well.

5.5 Full simulation

We conclude with a set of simulations where we simulate 500 machines with several types of concurrent misalignment, and we apply the beam based correction schemes. We now observe the total 3σ beam envelope (including macroparticle distribution and adiabatic damping), to verify whether the enitre beam can be transported . The machines simulated have the following initial misalignments (before correction):

- $\sigma_{PETS,x,y} = 100\mu$m

- $\sigma_{PETS-\theta,x,y} = 2$mrad

- $\sigma_{quad} = 20\mu$m

- $\sigma_{BPM} = 20\mu$m

- $\sigma_{res} = 10\mu$m

In Figure 18 we show the development of the beam envelope along the lattice (worst of all machines) for the uncorrected case, the 1-to-1 steered case and with dispersion free steering. We note that without beam based alignment the envelope exceeds the available aperture.
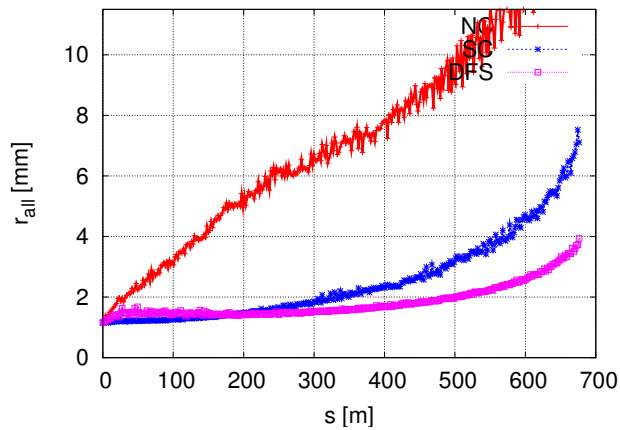

Figure 18: Full simulation of 500 machines

5.5.1 Histogram over the simulated machines

Figure 19 shows how the result of all machines are distributed for the simulation above. We see that without correction or with 1-to-1 steering there is a long tail of machines outside the 90% limit, while for dispersion free steering there is no significant tail.
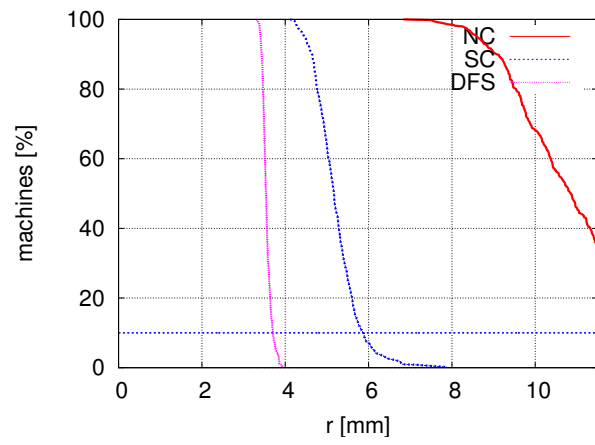
17

Figure 19: Distributions of all simulated machines

6 Conclusions

First, we conclude that the current PETS design, with the nominal parameters, gives sufficient damping of the transverse modes. However, if wake Q-factors or amplitudes are off by a factor two or more from the predicted values one can risk unacceptable mode amplification.

Furthermore, in this note we have sought to find the limits on the alignment tolerances resulting from lattice element misalignment. This has been performed by requiring transport of the entire beam through one decelerator station, for 90% of all machines, while achieving the required power extraction at an energy extraction efficiency of $\eta = 85\%$. We have shown that with adequate pre-alignment and the use of beam-based alignment, the effect of element misalignment can be well contained.

The corresponding tolerances are:

- PETS positioning misalignment : $\sigma_{PETS} \leq 100\mu$m

- Quadrupole initial positioning misalignment: $\sigma_{quad} \leq 20\mu$m

- BPM positioning misalignment: $\sigma_{BPM} \leq 20\mu$m

- BPM resolution: $\sigma_{res} \leq 10\mu$m

- PETS and quadrupole angle error tolerance : not tighter than $\sigma \leq 1$mrad

- Dispersion free steering with test-beams with e.g. missing bunches must be applied to the lattice, with initial 1-to-1 corrections (other beam-based alignment methods might be considered as well)

As final remarks, it should be underlined that the values for σ_{quad} and σ_{BPM} should preferably be even better than 20μm in order to avoid large losses during machine tune-up. On the other hand, this study doesn't result in very thight limits for the angle tolerances, but other effects not studied in this document might lead to tighter specifications for the angle error tolerances than found here.

7 Acknowledgements

References

[1] CLIC collaboration. The clic rf power source : a novel scheme of two-beam acceleration for electron-positron linear colliders. Technical report, CERN, 1998.

[2] A. Latina. private communication, 2007.

[3] D. Schulte. *The Tracking Code PLACET*, 2000.

[4] D. Schulte. https://savannah.cern.ch/projects/placet/. online, 2007.

[5] D. Schulte. private communication, 2008.

[6] D. Schulte, A. Latina, and P. Eliasson. Dynamic effects during beam-based alignment. In *PAC*, 2007.

[7] I. Syratchev, D. Schulte, E. Adli, and M. Taborelli. High rf power production for clic. In *PAC*, 2007.

A   Parameters

This appendix contains the parameters used for the calculations and simulations in this note. These parameters were up to date in the first half of 2007, but they might be subject to change in the future. For the beam envelope the most important parameters are the PETS parameters, the drive beam current and the initial energy, so if these parameters are not changed significantly the results should not change significantly either.

However, future notes and updates might use different parameters, and might therefore lead to different results than presented in this note.

A.1   Simulation set-up

The simulations are performed with PLACET 0.94, using 2nd order tracking of a sliced beam (a number of macroparticles with their $\Sigma - matrices$ are being tracked).

Each bunch is sliced into a number of slices in order to simulated the single bunch effects in a realistic manner. Tests shows that ~ 50 slices are needed before we converge.

The number of bunches simulated depends on what is being studied. The nominal train length is $240ns$ (~ 2800 bunches). This would result in a need for tracking ~ 140000 macroparticles, with distribution, something which will take a huge amount of simulation power even for one run through the lattice.

For the nominal PETS parameters the bunch train reached steady-state behaviour after 12 bunches, and therefore only 20 bunches are included in most of the simulations. All beam-based alignment simulations are performed with 20 bunches. Tests simulations with more bunches, and also weighting of the last bunch (to simulate the full train), did show that the result is not much different than for simulations with 20 bunches.

However, when the deviations from nominal PETS parameters are studied (large Q,w) a train length of $100ns$ is used in order to observe modes that grows along the train due to insufficient damping. E.g. all graphs showing plots with Q or w scaling has been performed with $100ns$ trains.

A.2   Lattice

		LATTICE PARAMETERS
$L_{unit}[m]$	0.986	Length of one unit (qpole and 2 PETS). Also length between two qpoles
$\mu_{x,y}$	90.1^o	FODO cell phase-advances
$L_{PETS}[m]$	0.231	Active length of one PETS
$L_{qpole}[m]$	0.15	Active length of qpoles
$L_{qpole_{tot}}[m]$	0.25	Total length of qpoles
$L_{BPM}[m]$	0.10	Length of BPMs
$L_{c-drift}[m]$	0.075	Length of cavity couplers
$L_{e-drift}[m]$	0.0	Total extra drift (*spare space*)
$k_{qpole}[m^{-2}]$	10.1	Normalized quadrupole strength (results in a phase advance of $\mu = 90°$)
N_{PETS}	1372	PETS
$a_0[mm]$	11.5	PETS half-aperture

The lattice used for these simulations consisted of 1372 PETS, contained in 343 FODO cells for a total length of $676m$. The real decelerators will have some, unevenely distributed, empty

slots between quadrupoles, and will be of length from $750m$ to $950m$. The difference in envelope growth in the short decelerator used here and the longer decelerators in the real design is shown to be not be very large.

A.3 PETS and power

|		PETS PARAMETERS
$\frac{R}{Q}[\frac{\Omega}{m}]$	1147	(Circuit-ohms; multiply by two for Linac convention)
β_L	0.4529	Longitudinal mode group velocity
$\lambda_L[m]$	0.025	Longitudinal mode wavelength ($11.99GHz$)
		BEAM PARAMETERS
$E_0[GeV]$	2.48	Initial beam energy
$n_{bunches}[m]$	50	Number of bunches in the beam (enough to reach ss)
$q_{bunch}[nC]$	8.0	Charge per bunch (5.0e10 particles)
$d[m]$	0.025	Distance between bunches
$I[A]$	96.0	Resulting current
$\sigma_z[\mu m]$	1000	Bunch rms length (Gaussian shape, cut at 3 σ)
$F(\sigma_z)$	0.967	Resulting form factor
$\{\varepsilon_{0,x}, \varepsilon_{0,y}\}[10^{-6}m]$	$\{150, 150\}$	Initial normalized emittance
		RESULTING POWER AND ENERGY
$P_{wo}[MW]$	149	Cavity steady state power output, w/o wall losses
$P[MW]$	147	Cavity steady state power output, w/ 1 % wall losses
$\Delta\hat{E}[MeV]$	1.63	Maximum deceleration per cavity in steady-state
$S = (1 - \frac{E_{min}}{E_{max}})[\%]$	90.0	Max final beam energy spread
$\varepsilon = S \times \frac{P[W]}{\Delta E_{PETS}[eV] \times I[A]}[\%]$	84.6	Power Extraction Efficiency coefficient (steady-state)

A.4 Transverse modes

	$w_T[V/m^2 pC]$	$Q[-]$	$f[GHz]$	$\beta[-]$
1	45	300	27.44	0
2	19	180	28.05	0
3	17	290	32.9	0
4	200	85	39.12	0
5	30	120	41.8	0
6	15	380	48.9	0
7	850	3.7	10.0	0
8	4820	3.8	13.4	0
9	2630	6.2	15.46	0

Modes are modelled with $\beta = 0$ for all modes, and a correspondingly lower Q-factor ("equivalent Q") is used.

## A.5 Comment on the number of machines simulated

For most of the simulations in this note where rms values are given for misalignment, 100 machines have been simulated (and not more, mainly due to simulation computer time).

Below we show how 100 machines are distributed with respect to 10000 machines for the case of $\sigma_{PETS} = 100\mu$m and no correction.

100 machines versus 10000 machines
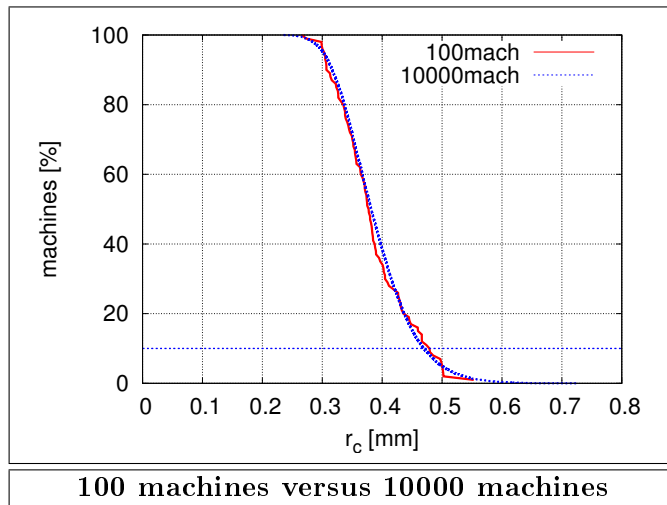
We note that 100 machines give a fair impression of the distribution, with the exception of the longer tail for the 10000 machines.

Below we plot the 10000 machines in a log-plot, and we observe a steep drop in the curve as more machines are in included. This indicated that the metric used in this note, by using 90/100 machines will give a number that is not very far off the value one gets by defining a stricter metric and larger statistics (e.g. since we have $\backsim$ 50 decelerators one would ideally require 9980 of 10000 machines in order to have a 90% probability of each decelerator adhering to the requirements).

10000 machines
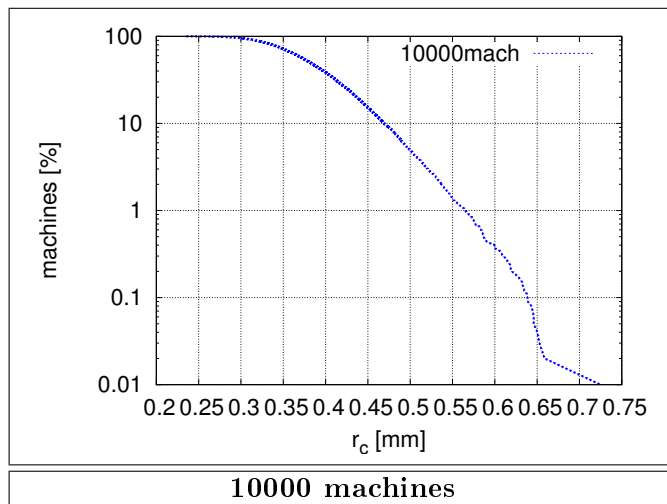
# B Summary of the impact of the PETS transverse wake fields

This appendix summarizes the effects of the PETS transverse dipole modes on the drive beam for the CLIC decelerator.

The PETS transverse wake is modelled as 9 dipole modes, each characterized by $\{f_{T,i}, w_{T,i}, Q_{T,i}\}$ ($\beta_T = 0$ for all modes in this model).

All results are shown for the full CLIC decelerator lattice. The pulse length simulated is $100ns$ (the nominal pulse length is $240ns$ but $100ns$ is considered long enough to see the significant effects, and is used since $240ns$ requires a much larger amount of computing resources).

B.1 Amplification of single modes (centroid)

The amplification of each mode is studied by using an initial beam, offset with a transverse frequency corresponding to one individual mode, and comparing the final centroid envelope without any wakes ($w_T = 0$) with the final centroid envelope with wakes included. The results are shown below for both nominal and scale Q factors.


Amplification of single modes - CLIC (100 ns)
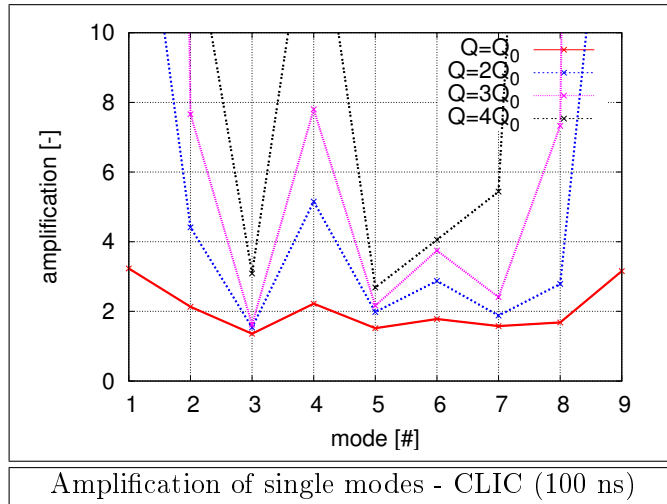
B.2 Amplification of combined modes jitter (centroid)

In simulations it can be useful to to use a beam which includes frequencies of all the transverse modes simultaneously, in order to verify that beam jitter does not blow up the beam too much. A beam offset with frequencies of all the 9 modes super-positioned is amplified by the amount shown below, for various $Q - values$.

CLIC - Q-scaling centroid
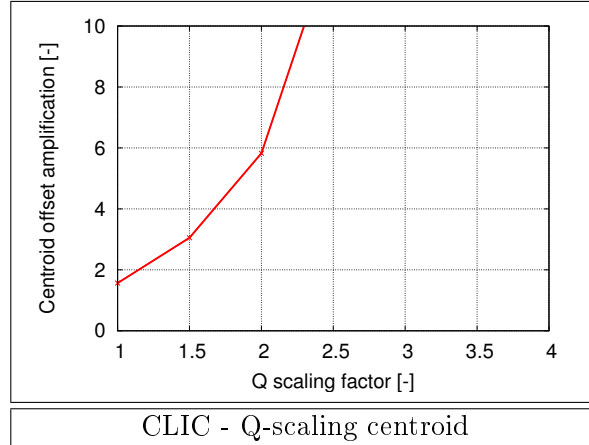
B.3 1σ jitter om top of beam envelope (total envelope)

The following plots shows the relative effect of incoming jitter on all frequencies on the *total* 3σ beam envelope (including macroparticle distribution and adiabatic undamping). The incoming jitter has a total of amplitude 1σ ($\sim 35\mu$m amplitude for each mode). This way of calculating the amplification is less conservative, but in some ways more realistic, than looking only at the centroid amplification as in last section.


CLIC - Q-scaling   CLIC - w-scaling
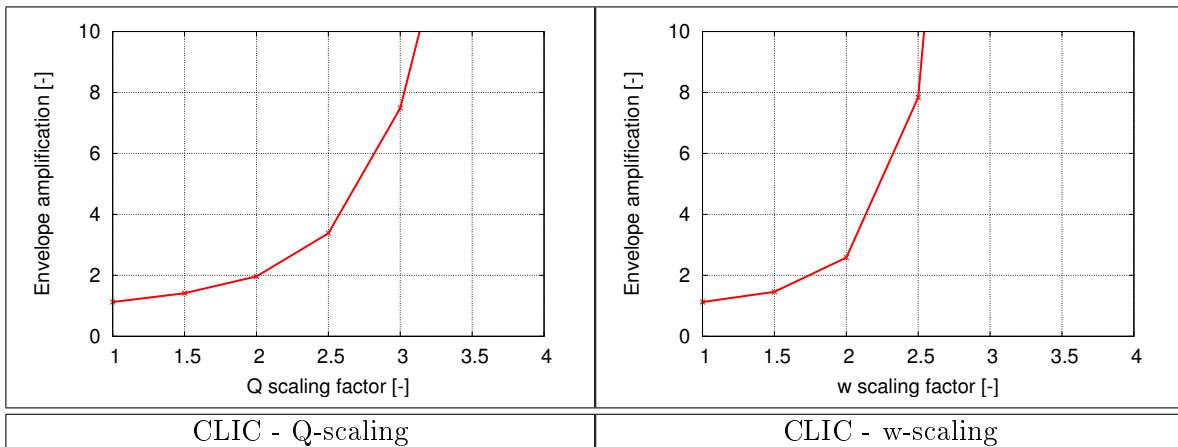
Further examination

The following graphs show how the 3σ beam envelope described in the last section evolves along the lattice progresses, as well as examples of how the resulting final beam would look like (again for cases of zero-wake, nominal Q and scaled up Q). It is seen that for $Q = 2Q_0$ slowly growing modes with large amplitudes are introduced in the beam, so Q-factors twice higher than the nominal would be considered unacceptable.

CLIC (100 ns)

CLIC Q=w0 (100 ns)

CLIC Q=Q0 (100 ns)

CLIC Q=2Q0 (100 ns)

CLIC Q=3Q (100 ns)
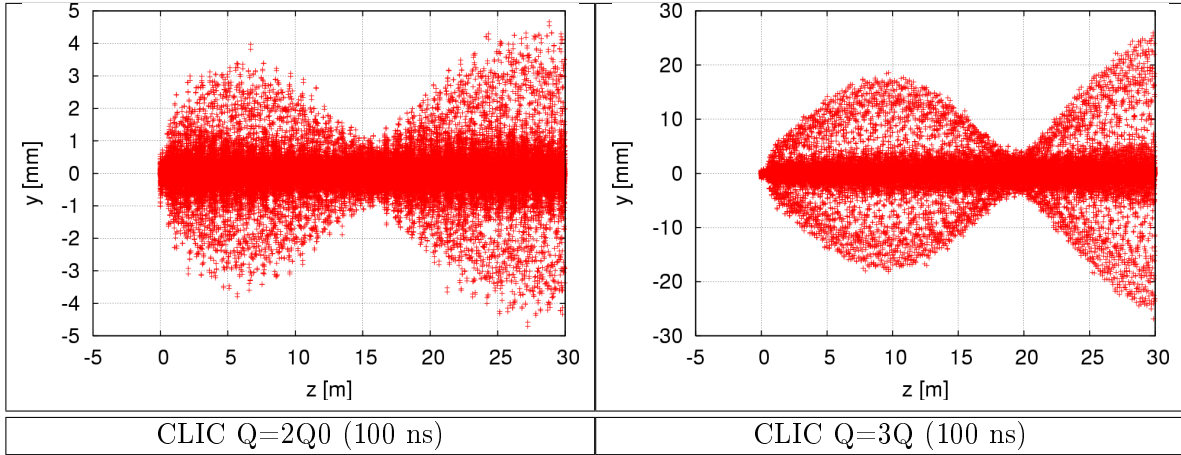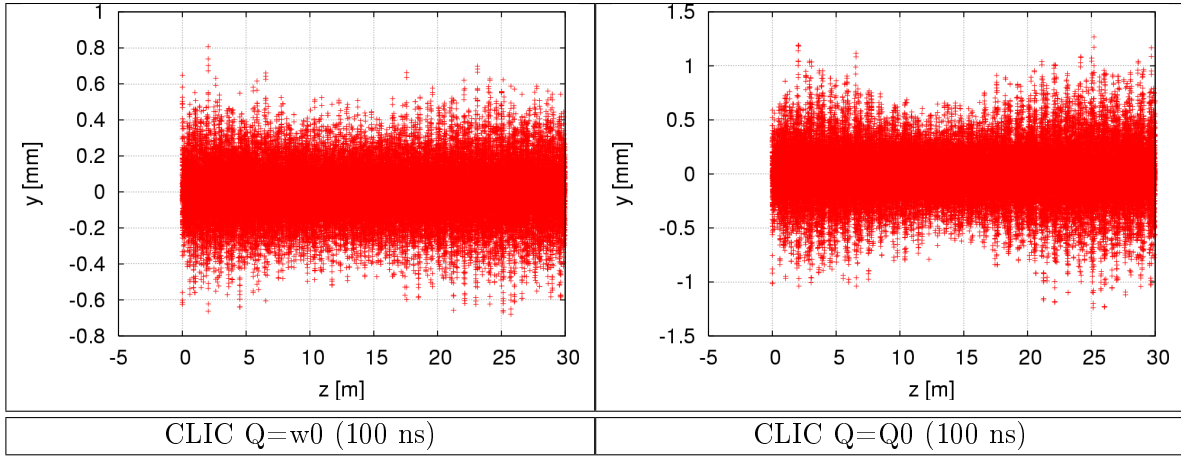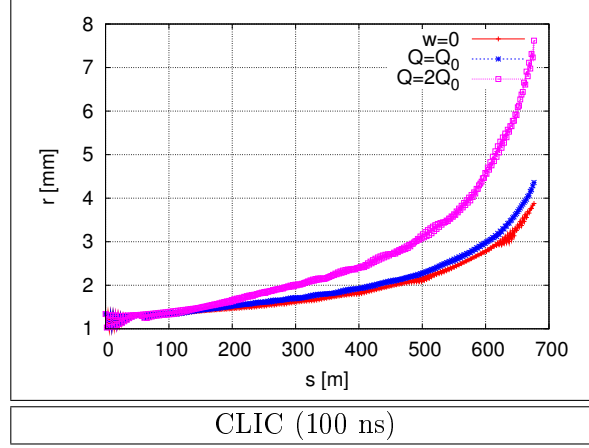
B.4 PETS scatter and perfect incoming beam (centroid)

The following graphs shows the result when the incoming beam is perfect (no jitter), but the PETS are scattered randomly with a given σ_{PETS}. Results corresponds to 90 out of 100 simulated machines. We see, as expected, as the PETS wake amplification is nowhere as drastic when we do not induce jitter with the exact PETS dipole mode frequencies.
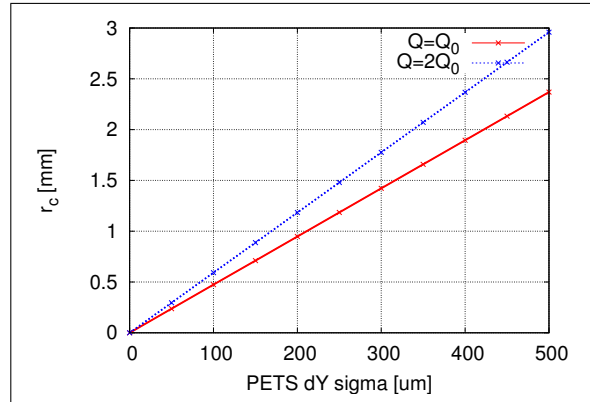
PETS jitter - CLIC

C   Details about the dispersion free steering

The dispersion free steering was performed with one test beam (reduced current by removing 1/3 of the bunches). Two test beams did not give significantly better results.

The bin-length was 48, and the bin overlap was 24.

Only one iteration was needed, due to the linear lattice.

All simulations were run with $w_1/w_0 = 100$. As shown from the plot below, this is optimal for $\sigma_{res} = 2\mu$m, and also very good up to $\sigma_{res} = 18\mu$m.

Dispersion Free Steering weights

Main beam and test beam energy

Alternative test beam
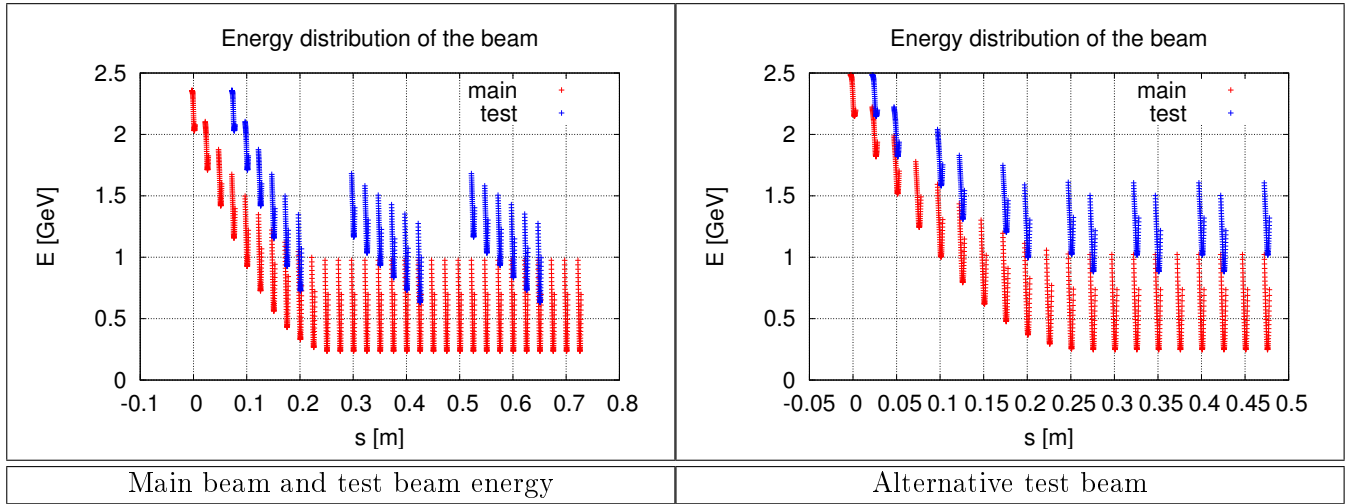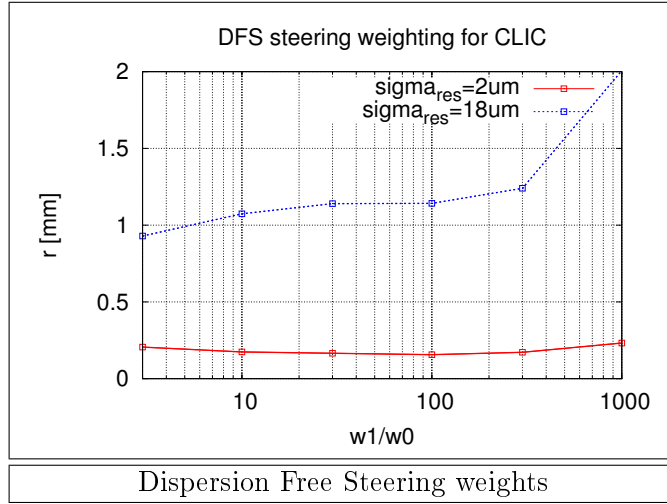
C.1   Aligning quadrupoles with the PETS off

It is foreseen that the PETS will be equipped with wedges ("Petsonov") that will effectively set the impedance to zero. With the PETS off, one could perform DFS using a lower-energy beam as test-beam, as for the main linac. This has the advantage that without adiabatic undamping and wake field kicks, the beam envelope will be smaller, and lower tolerance will be required for the initial quadrupole alignment. However, with nominal current and full energy the beam will be more dangerous to the machine and the dump. On the other hand, running the alignment

procedures with low intensity beams has the disadvantage that the calibrations might not be the same in this regime.

This suggests that the preferred alignment solution will still be to keep the PETS kept on and use the reduced-current test beam. In the DFS simulations performed we have thus used the nominal current, and the nominal a decelerator lattice with the PETS on.

C.2   Analysis of the effect of DFS

It should be noted that even though DFS can be very effective in reducing the envelope (and emittance) growth along the lattice, it doesn't necessarily lead to a better rms spread of the quadrupole position. In most cases simulated below the rms spread actually increases.

In the ideal case, with perfect BPMs, the algorithm would align the quadrupoles perfectly. However, for finite BPM resolution and the weighting scheme above, only the harmful modes of the quadrupole spectrum that will be reduced. This is shown by doing a Fourier analysis of the quadrupole positions before and after alignment. This has been performed for one particular machine, shown in below .
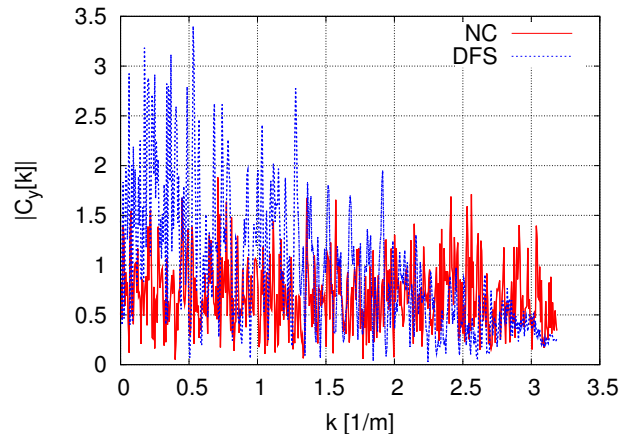

Figure 20: Spectrum of quadrupole position, before and after DFS

It clearly shows that after correction, harmful correlations corresponding to closely spaced quadrupoles are suppressed, while large distance correlations are increased. The case simulated is one machine, with $\sigma_{BPM} = 20\mu$m, $\sigma_{res} = 0.1\mu$m. Before correction $\sigma_{quad} = 10\mu$m, while after correction, $\sigma_{quad} = 15\mu$m.